Temperature and grain size effects on the behavior of CuAlBe SMA wires under cyclic loading

Rodrigo Araya, Marco Marivil, Cristóbal Mir, Ofelia Moroni*, Aquiles Sepúlveda

Universidad de Chile, Facultad de Ciencias Físicas y Matemáticas, Beaucheff 850, Santiago, Chile

A B S T R A C T

This study evaluates the properties of a superelastic CuAlBe shape memory alloy under cyclic loading to assess its potential for applications in seismic resistant design. Wires $\phi = 0.5$ mm, previously heated during different periods of time, are tested to study the effect of grain size, temperature and strain rate on the strength, equivalent viscous damping, and recentering properties of the alloy. The wires are subjected to quasi-static and dynamic tensile loading tests. The results show that nearly ideal superelastic properties can be obtained up to 3% axial strain. Overall, the damping potential of the alloy is moderate, typically less than 5%. Increased temperatures lead to a reduction in the equivalent damping and an increase in the forward transformation stress, and increased grain sizes lead to an increase in the equivalent damping and a reduction in the forward transformation and ultimate stresses.

Keywords:
Shape memory effect
Grain size
Cyclic tests
Equivalent viscous damping

1. Introduction

Shape memory alloys are materials that can exhibit large strains under loading–unloading process without residual deformation. Depending on the working temperature, the removal of deformations induced by stress may require unloading and heating (shape memory effect) or simply unloading (superelasticity). Both effects are closely related to the martensitic transformation, which is a diffusionless solid-state one where atoms move cooperatively (military), often by a shear-like mechanism [1]. Even though the relative atomic displacements are small, compared with interatomic distance, a macroscopic shape change appears connected with martensitic transformation. It involves a high-temperature parent phase, austenite or phase β, with high symmetry, and a low-temperature metastable phase, martensite, with low symmetry. Although many variants of martensite can be formed from an austenitic single crystal, during the reverse transformation all the variants lead to the same parent phase. The variants have the same crystalline structure, and they only differ on the relative orientation.

When rapid cooling is applied to the material at a temperature where β phase is stable, the resulting austenite is metastable. For lower temperatures, the metastable martensitic phase appears. Superelasticity is possible only if the austenite is metastable; so that stress-induced martensite can form. This requires that temperature must be higher than A_f, the austenite finish phase transformation temperature. Initially, when loads are applied, metastable austenite is deformed elastically until the forward transformation stress (σ_t) is attained, starting a non-linear stress–strain relation afterwards. When unloading, the phase transformation reverses and the material recovers its original shape. In tensile tests, reversible non-linear strains between 2 and 8% can be attained and energy dissipation occurs through hysteresis cycles.

When the working temperature is increased, σ_t increases, because the parent phase is more stable. Above the limit temperature, M_D, pseudoelasticity is not possible due to austenite stability [1]. Also there is a maximum strain after which strains are no longer reversible; this limit is lower for a polycrystalline material than for single crystal. The grain size has an effect on the phase transformation temperatures and on the shape of the hysteresis cycles and therefore, on the energy dissipation capacity.

Most of the previous research involves TiNi alloys or Cu- and Fe-based alloys due to their potential or effective technological applications. Thorough reviews concerning potential uses of Ni–Ti based SMAs in earthquake engineering can be found in DesRoches and Smith [2], Song et al. [3], and Wilson and Wesolowsky [4]. They include state of the art information about modelling, design and testing of devices, as well as analytical and experimental studies on their use in buildings and bridges.

In particular, Cu-11.8 wt.%Al–0.5 % wt.%Be alloy has shown pseudoelasticity at room temperature, and may be used in seismic energy dissipation devices for civil structures [5,6]. Other requisites for SMAs to be used in seismic devices are high fatigue resistance, low sensitivity to temperature in the 5–35 °C range, low sensitivity

* Corresponding author. Tel.: +56 2 9784698; fax: +56 2 6892833.
E-mail address: mmoroni@ing.uchile.cl (O. Moroni).

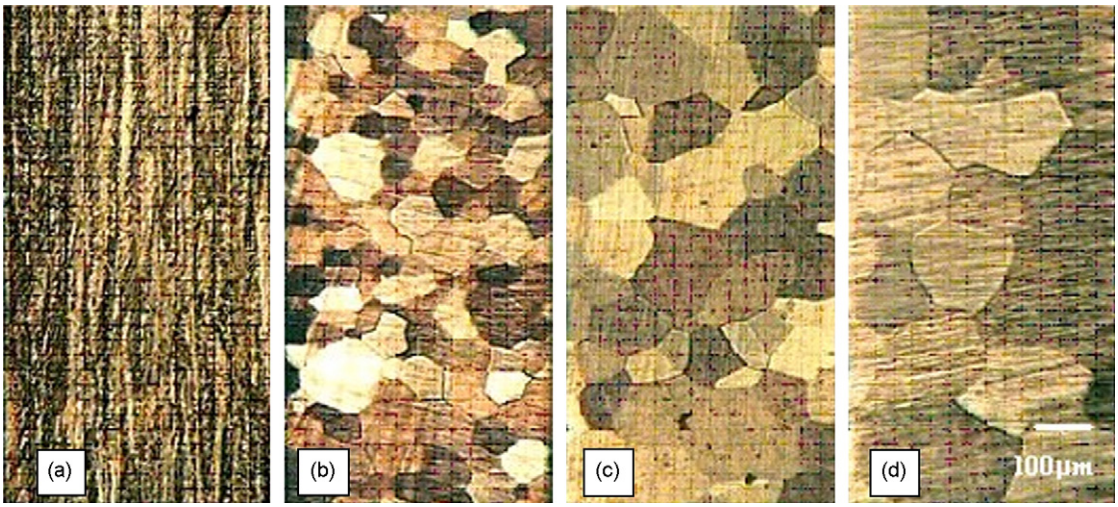

Fig. 1. Longitudinal optical metallographies: (a) original material. (b) Heat treatment at 700 °C during $t = 20$ s, resulting in $d = 63$ μm, (c) 30 s and 98 μm and (d) 180 s and 196 μm.

to frequency in the 0.1–5 Hz range and no or slow degradation due to environmental actions.

This study evaluates the properties of a superelastic CuAlBe shape memory alloy under cyclic loading to assess its potential for applications in seismic resistant design. Wires 0.5 mm diameter, previously heat-treated during different time periods, are tested to evaluate the effect of grain size (60–300 μm), temperature (6, 20, 25 and 50 °C) and strain rate on the strength, equivalent damping, and recentering properties of the alloy.

2. Experimental procedure

Wires, $\phi = 0.5$ mm diameter, with nominal composition Cu-11.8 wt.%Al–0.5 wt.%Be, furnished by Trefimétaux, France, were tested under both quasi-static and dynamic tensile loading. Phase transformation temperatures reported by the manufacturer are $M_f = -47$ °C, $M_s = -18$ °C, $A_s = -20$ °C and $A_f = 2$ °C. Since ambient temperatures for civil engineering structures are usually greater than the A_f transition temperature of 2 °C, the material is expected to operate within its superelastic range.

The initial microstructure showed long elongated grains and high reactivity to metallographic attack, Fig. 1(a), associated to severe longitudinal deformation due to cold work. After thermal treatment at 700 °C for different time periods, t, followed by iced-water quenching and ageing at 100 °C for 24 h, different average grain sizes were obtained. Fig. 1(b–d) shows longitudinal optical metallographies of 120 mm long wires, for different heating time periods: $t = 20$ s ($d = 63$ μm), $t = 30$ s, ($d = 98$ μm) and $t = 180$ s ($d = 196$ μm), respectively. As verified by longitudinal and transverse optical microscopy observations, grains appeared as basically equiaxial after heat treatment. In the previous heat-treated samples the ratio d/ϕ was equal to 0.126, 0.196, and 0.392, respectively. Grain size was determined using the line intercepted method, with at least 100 intercepts by sample. The statistical error of the average grain size calculation, with 95% reliance, was always less than 10%, for the small and medium grain size and less than 15%, for the larger grain size.

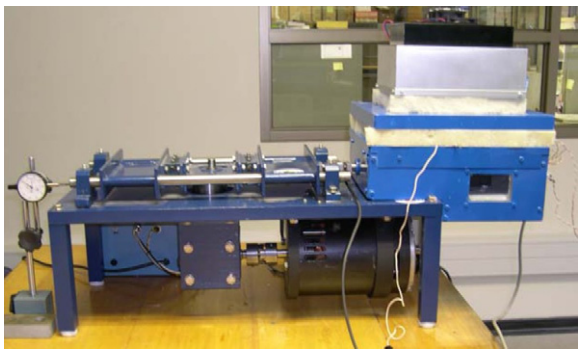

Fig. 2. Equipment for monotonic and cyclic tensile tests.

Static and cyclic tensile tests were performed. A machine, originally designed to test rubber samples in shear [7], was modified for testing wires subjected to tensile force, Fig. 2. The frequencies used for these tests varied between 0.03 and 1.0 Hz. An imposed sinusoidal displacement is obtained by rotation of an eccentric shaft and two sliding guides. The amplitude of motion is controlled by changing the eccentricity of the shaft. The device has a mechanical system that allows for different displacement amplitudes. Active elements used for the heating and cooling system consist of two Peltier thermo-electrical cells of 80 W each. These cells produce a temperature differential between two faces when connected to an electrical DC source. The system can be used either for heating or for cooling of a specimen, just by inverting the polarity of the source. The specimen is located inside a plastic-foam isolated box with one perforation for the loading rod. There are also two heat exchangers, one internal and another external, that are connected to the thermo-electrical cells. Finally, internal and external electrical fans aid in the heating and cooling process and also in the homogenization of the internal temperature. The temperature level is controlled by means of an electronic thermostat. The precision obtained for the temperature of the specimen is ±1 °C.

The test samples were 90 mm long, while the distance between the machine grips was about 70 mm. The cyclic tests were performed for nominal strain amplitudes of 0.8, 1.5 and 2.2% and for temperatures ranging from 6 to 50 °C. The strain was measured with an extensometer that has a 25 mm gauge length. The wires were initially slightly prestressed to avoid buckling. Each sample was tested at one amplitude with the following temperature sequence 25, 6, 50, 25, 6 and 50 °C. Later, some samples were retested at 25 °C up to fracture. Most of the tests consisted of series of 20 cycles at defined nominal strain amplitudes. To observe the evolution of the hysteresis cycles, some of the series included up to 60 cycles.

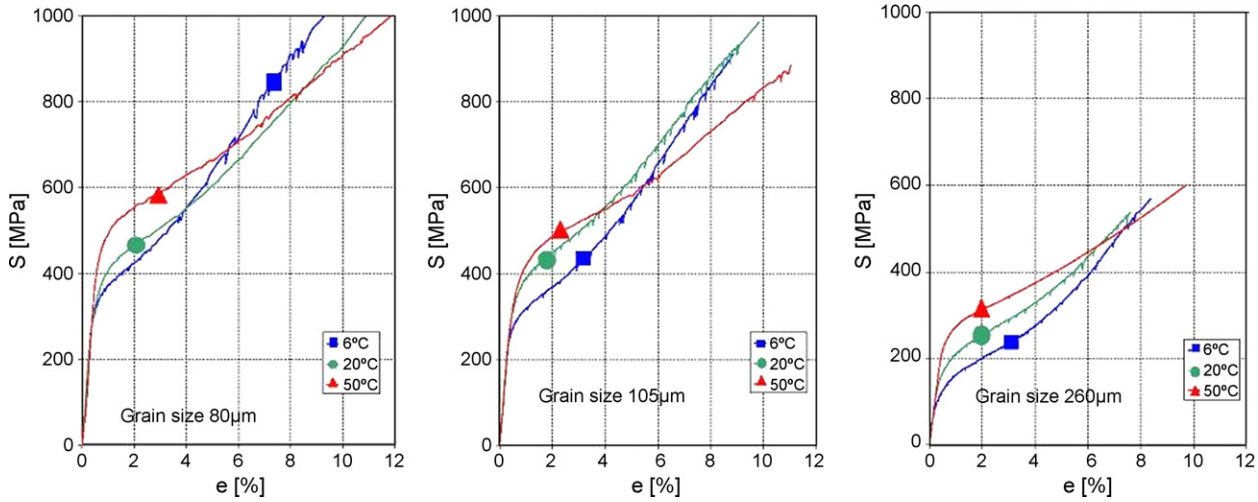

Fig. 3. Monotonic stress–strain curves at different temperatures (▲ 50 °C, ● 20 °C, ■ 6 °C) and for various grain sizes (80 µm, 105 µm, 260 µm).

3. Results and discussion

3.1. Monotonic tensile tests

Fig. 3 shows the monotonic stress–strain curves up to fracture for samples of three grain sizes tested at 6, 20 and 50 °C. The general shape of each of these curves is similar to that previously observed for other specimens of the same superelastic material [5] (a) first, a linear region corresponding to classic austenitic elastic deformation, (b) then a second region, properly corresponding to the superelastic behavior, presenting stiffness degradation followed by a linear stress–strain relationship, and (c) finally, another roughly linear region, culminating in a fracture point, with a slope slightly higher than that of the previous superelastic region. The stress limit of the first region corresponds to the forward transformation stress, σ_t, which is the minimum stress in loading that permits the initiation of the austenite-into-martensite stress-induced transformation. This stress was measured from the tensile curves using the same definition as for the classic conventional elastic limit for a deformation of 0.05%. The martensitic transformation finished for 4–8% strains, after that a hardening effect is observed.

Fracture took place near the tensile clamps, meaning that it actually initiated under a complex stress state. Thus, the fracture stress values observed in curves of Fig. 3 are lower limits in reference to fracture stress under uniaxial-tensile-stress conditions. Slight reduction of the cross-section area was noted only for the largest grain-size wire. Scanning electron fractographies, not shown here, revealed a transgranular fracture with coexisting zones of dimpled and cleavage characteristics; similar observations have been previously reported for tensile specimens of this alloy [6].

Table 1 presents the values obtained from the above curves for the Young Modulus, E, the forward transformation stress, σ_t, the ultimate tensile stress (σ_u), and the strain corresponding to σ_u, e_{UTS}. The following observations and comments can be derived from Fig. 3 and Table 1.

- For a given grain size, σ_t increases when temperature increases. This is consistent with the fact that at higher temperatures austenite is more stable, and so a larger stress is required to start the martensitic transformation.
- On the other hand, for a given temperature, σ_t increases when grain size decreases. It has been previously reported that σ_t follows a Hall-Petch type tendency, which can be ascribed to grain boundaries acting as barriers to martensitic shearing [8].

Table 1
Static tensile results

Grain size, d (µm)	Temperature, T (°C)	E (GPa)	σ_t (MPa)	σ_u (MPa)	e_{UTS}[a] (%)
80	50	89.5	378	1022	10.4
	20	113.3	266	1018	12,3
	6	100.5	254	1037	8.9
105	50	72.4	281	900	9.8
	20	78.3	247	984	8.7
	6	101.4	217	910	7.8
260	50	48.7	206	600	9,7
	20	42.5	129	530	6.4
	6	30.8	89	568	6.5

[a] Length: 25 mm.

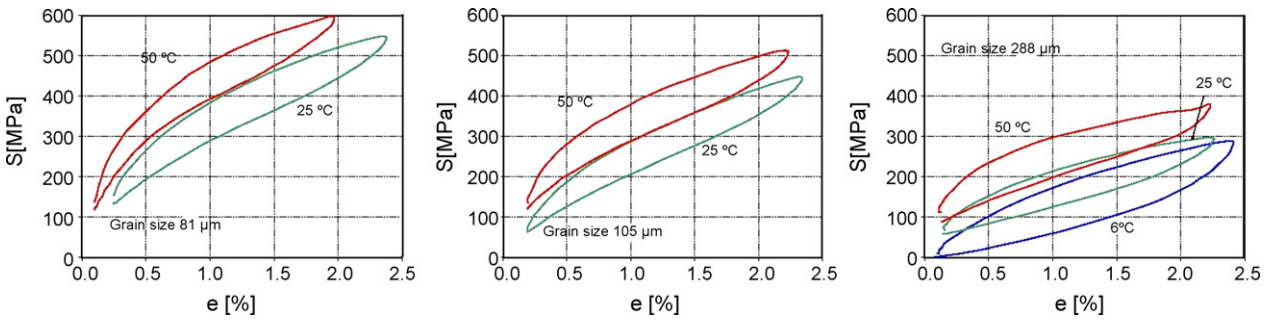

Fig. 4. Cyclic stress–strain curves at different temperatures: 6, 25 and 50 °C. Each graphic corresponds to a grain size; from left to right: 81, 105 and 288 µm.

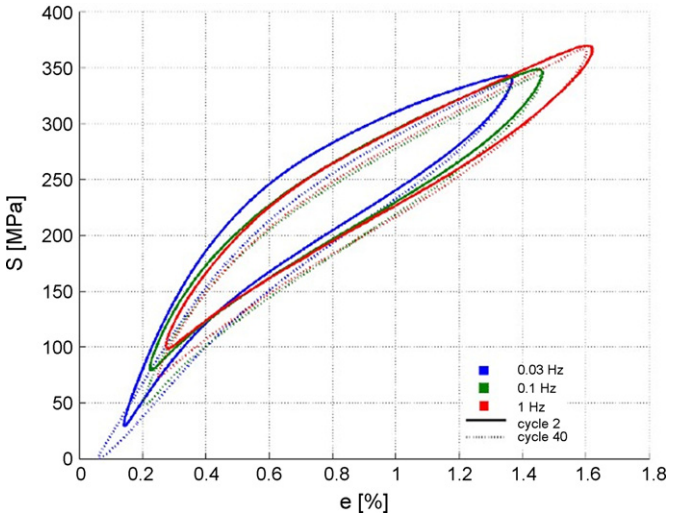

Fig. 5. Stress–strain curves for cyclic test at different frequencies, $d = 115$ μm.

- Young modulus diminished as the grain size increased.

Note that the above also applies for the effect of temperature and grain size on the flow-stress curves in the superelastic region. With respect to the fracture point, it is observed that σ_u and e_{UTS} increase as grain size decreases; moreover, there is no clear influence of temperature on σ_u and e_{UTS}. This behavior agrees with the fact that fracture point corresponds to a condition where the total or a significant fraction of the gage volume of the pertinent tensile specimen is already in martensitic phase and, accordingly, not in an essentially superelastic state, but rather in a classical one.

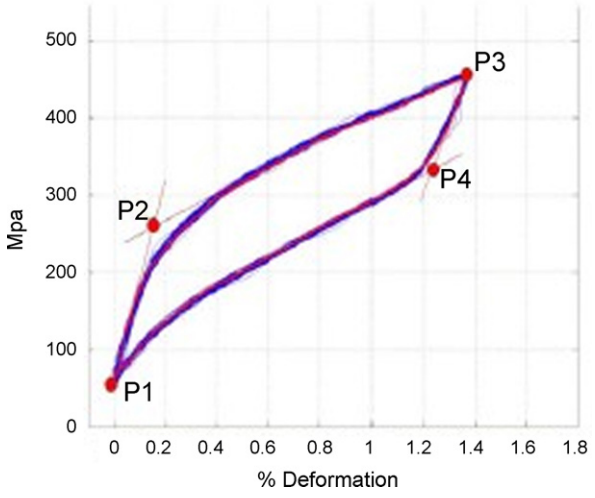

Fig. 6. Phase transformation stresses.

Previous cyclically tested wires showed, in monotonic tests, similar behavior with respect to grain size and temperature than those mentioned before. However, in previously cycled samples transformation stresses are about 40% lower.

3.2. Cyclic tensile tests

Fig. 4 shows cyclic tensile curves obtained for a nominal strain amplitude of 2.2% at 1 Hz, and for different grain sizes and temperatures. In each case, series of 20 cycles were imposed; for clarity sake only the stress–strain of the second cycle is given; actually, the first cycle was somewhat different from the others, while all the rest are very close to each other. According to Somerday et al. [9], modest plasticity is thought to occur in the first loading cycle. Anomalous first cycles have been also observed in another CuAlBe polycrystals [8]. We here propose a complementary explanation, valid for our experimental conditions, which is associated to the use of a prestrain in tensile cycling tests where the stress–strain loops present a "flag without rope" shape, see Fig. 4. In effect, under such conditions, even for a perfectly superelastic material, the second cycle should start, at minimum strain, from a smaller stress than that of the first cycle. Finally, for the application of superelastic devices as seismic dampers, some difference between the first cycle and the following homogeneous ones should be negligible, as the number of cycles in an earthquake is typically bigger than 20.

The following remarks can be drawn from cyclic tests:

- The material shows superelasticity. Actually, within experimental strains error limits, no residual deformations were detected under the employed tests conditions, although retained martensite was observed in optical microscopy images taken after the tests and not shown here.
- For a given grain size, σ_t and the effective stiffness increase for increasing temperatures. The effective stiffness, a relevant civil-engineering design parameter, is defined for each cycle as the ratio $(\sigma_{max} - \sigma_{min})/(\varepsilon_{max} - \varepsilon_{min})$.
- Effective stiffness and forward transformation stress decrease for larger grain size.
- For a given grain size, the maximum stress increases and the maximum strain diminishes as temperature is increased. This behavior is related to the effect of temperature on the flow stress curve and to the type of strain control used in the tests. As it was pointed out, for higher temperature the material is stiffer, therefore, for the same load, less deformation is attained. Note that the system machine-wire can be modelled as two springs in series, with a unique imposed total deformation. For a constant imposed deformation, the stiffer the wire (considering it as a spring), the smaller will be the wire deformation and a larger load will be needed to deform it.

Fig. 5 shows the second and fortieth cycles of wires with $d = 115$ μm, tested at 0.03, 0.1 and 1 Hz at 25 °C, and for 1.5% nominal strain

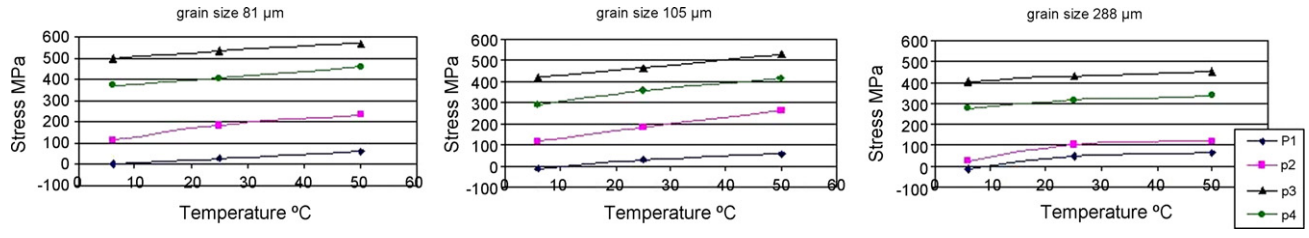

Fig. 7. Start and finish transformation stresses for 2.2% strain amplitude as a function of temperature, as obtained from data contained in Fig. 4.

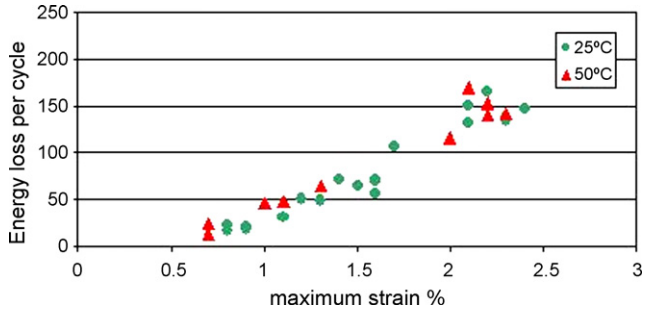

Fig. 8. Energy loss per cycle as a function of maximum strain, for different temperatures.

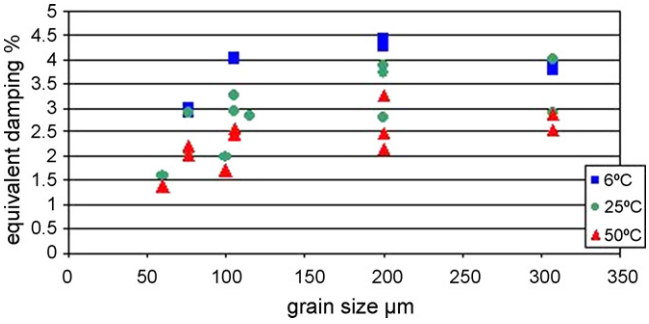

Fig. 9. Equivalent viscous damping as a function of grain size, for different temperatures.

amplitude. It can be seen that, test frequency has only a slight effect on hysteretic cycles.

For each temperature, the critical stresses associated to the forward and the inverse phase transformation in cycle tests were evaluated; it was assumed that these stresses coincide with the ordinates of the intersection points between the tangent lines shown in Fig. 6 (P_2 and P_1, respectively). Based on these values, the starting and completing transformation lines were drawn in Fig. 7 for a 2.2% strain amplitude, and for wires with 81, 105 and 288 μm grain sizes. It can be seen that their trend is linear, with an average slope of 1.6 ± 0.6 MPa/°C, significantly smaller than those obtained for Nitinol by Dolce and Cardone [10]. Transformation temperatures in the stress-free state can be estimated at the intersection points between the aforesaid lines and the horizontal axis. In this case, A_f values between 5 and 10 °C are obtained, the lower value corresponding to the smaller grain size.

With respect to dissipation parameters:

- The energy loss per cycle, corresponding to the stress–strain cycle area, increases as maximum strain increases and it seems independent of grain size and temperature, see Fig. 8.
- The strain energy (area under a loading cycle) decreases for larger grain sizes and increases when temperature increases.

Fig. 9 shows the equivalent viscous damping, calculated as the energy loss per cycle divided by (4π maximum strain energy per cycle) [11], as a function of the grain size for 2.2% nominal strain amplitude. For all grain sizes, a smaller equivalent damping is obtained for higher temperatures; moreover, damping is larger for larger grain sizes.

The above reported tendencies about temperature influence on dissipated and strain energy, and on equivalent viscous damping, are similar to those reported by Gil and Guilemany [12] for superelastic CuZnAl alloys with A_f between 13 and 25 °C, and tested in tension at temperatures between 10 and 70 °C. On the other hand, Dolce and Cardone [10] found, for a NiTi alloy subjected to cyclic tension, that the hysteretic cycle area depends slightly on temperature and that equivalent damping decreases for increasing temperature.

Passive damping includes the direct conversion of mechanical energy into heat by the material that is directly subject to vibrational or impact loading [13]. Damping occurs by the hysteretic movements of crystalline defects; therefore, the damping capacity is related to the hysteretic movement of interfaces (martensite variant interfaces, twin planes, martensite–beta interfaces) although a contribution of dislocations is not excluded. During pseudoelastic loading, for strain amplitudes beyond 10^{-2} the size of the hysteretic stress–strain loop is a measure for the damping capacity [13].

4. Conclusions

The mechanical behavior of Cu-11.8 wt.%Al–0.5 wt.%Be wires with different grain sizes (60–300 μm) has been tested in monotonic and cyclic tensile test at different temperatures (6, 20, 25 and 50 °C), frequencies (0.03, 0.1 and 1 Hz) and strain amplitudes (0.8, 1.5 and 2.2%).

1. Monotonic tensile tests showed that:
   (a) Forward transformation stress increased when temperature increased.
   (b) Forward transformation stress, maximum stress and maximum strain increased as the grain size decreased.
2. Cyclic tensile test showed that:
   (a) The material showed superelastic behavior.
   (b) Forward transformation stresses diminished as the temperature decreased and as the strain amplitude and the grain size increased.
   (c) The influence of the test frequency on the stress–strain curves was negligible.
   (d) Equivalent damping increased for larger strain amplitudes and larger grain sizes, and decreased for higher temperatures. For 2.2% strains, damping varied between 3 and 5%.

Acknowledgements

Funding for this study was provided by Universidad de Chile and by Fondecyt No. 1030554 and No. 1070370 grants.

References

[1] K. Otsuka, C.M. Wayman (Eds.), Shape Memory Materials, Cambridge University Press, Cambridge, 1998.
[2] R. DesRoches, B. Smith, Journal of Earthquake Engineering 8 (3) (2004) 415–429.
[3] G. Song, N. Ma, H. Li, Engineering Structures 28 (9) (2006) 1266–1274.
[4] J.C. Wilson, M.J. Wesolowsky, Earthquake Spectra 21 (2) (2005) 569–601.
[5] S. Montecinos, M.O. Moroni, A. Sepúlveda, Materials Science and Engineering A 419 (2006) 91–97.
[6] A. Sepulveda, R. Muñoz, F.C. Lovey, C. Auget, A. Isalgue, V. Torra, Journal of Thermal Analysis and Calorimetry 89 (1) (2007) 101–107.
[7] A. Escandar, M.O. Moroni, M. Sarrazin, P. Roschke, Journal of Materials in Civil Engineering 19 (5) (2007) 428–436.
[8] S. Montecinos, A. Cuniberti, A. Sepúlveda, Materials Characterization 59 (2) (2008) 117–123.
[9] M. Somerday, R.J. Comstock, J.A. Wert, Metallurgical and Materials Transactions A 28A (1997) 2335–2341.
[10] M. Dolce, D. Cardone, International Journal of Mechanical Sciences 43 (2001) 2657–2677.
[11] A.K. Chopra, Dynamics of Structures: Theory and Applications to Earthquake Engineering, Prentice-Hall, Upper Saddle River, NJ, 2001.
[12] F.J. Gil, J.M. Guilemany, Thermochimica Acta 290 (1997) 167–171.
[13] J. Van Humbeeck, MANSIDE Project (1999) II9–II44.